A NEURO-FUZZY BASED COMBUSTION SENSOR FOR THE CONTROL OF OPTIMAL ENGINE COMBUSTION EFFICIENCY

by

Nenad L. MILJIĆ* and Miroljub V. TOMIĆ

Department for Internal Combustion Engines, Faculty of Mechanical Engineering,
University of Belgrade, Belgrade, Serbia

Original scientific paper
DOI: 10.2298/TSCI120703160M

Modern and advanced control systems for internal combustion engines require accurate feedback information from the combustion chamber. Whereas the in-cylinder pressure sensor provides this information through its close thermodynamic ties with the combustion process, drawbacks in its implementation push research towards other non-intrusive sensing methods. This paper suggests alternative methods of combustion phasing detection relying on measured angular crankshaft speed. Method developed, achieves sensing of angular position of the 50% of mass fraction burned (MFB50) through two steps: calculation of, so called, synthetic torque and its non-linear transformation to a combustion feature estimator through localmodel. In order to calibrate both parts of this virtual combustion sensor, parameters of a high-fidelity crankshaft dynamic model are identified, and the linear neuro-fuzzy based model is trained with extensive experimentally collected data set. Created virtual MFB50 sensor, demonstrated its performance, on a large test data set comprised of 70% of gathered data.

Key words: *neuro-fuzzy, combustion sensor, internal combustion engine efficiency, Lolimot, MFB50, spark advance*

Introduction

The internal combustion (IC) engine is the dominant propulsion technology of the present and will be hardly possible to be completely replaced in the following decades. Relying on fossil fuels, IC engines, in road transport, are responsible for 16.8% of the world's CO_2 emission [1]. In the scope of Earth's climate change and increasing energy demands, more worrying is the fact that this emission has increased almost 50% in the last 20 years [1]. Research in the field of IC engines is, more than ever, focused on its efficiency improvement and emission reduction toward fulfilment of CO_2 targets already defined in regulatory frameworks worldwide [2].

Today's IC engine efficiency is close to 80% of a thermodynamically ideal engine. Missing difference is related to real process influences like heat losses, finite combustion duration, exhaust and blow down losses, crevice effects, leakage and incomplete combustion [3]. Comprehensive study on the factors influencing the extraction of maximum useful work from the IC engine working cycle can be achieved through exergy (availability) analysis. A survey, done by Rakopoulos and Giakoumis [4], on publications concerning the application of the second-law of thermodynamics to IC engines, gives detailed insight on parameters and strategies, which could lead to efficiency increase by minimising exergy destruction. Teh *et al.* [5] con-

* Corresponding author; e-mail: nmiljic@mas.bg.ac.rs

cluded that the internal energy state at the start and at the end of combustion have a very important role in minimising exergy destruction, giving sound explanation of significance of angular position of the combustion process within the engine working cycle.

It is well known that the spark advance is one of the key parameters of the spark ignition (SI) engine performance. Phasing the start of combustion influences the combustion process itself and largely influences the amount of work, which can be extracted from the working cycle. Maximum brake torque (MBT) can be achieved by optimally phasing the combustion process, *i. e.* by setting the optimal spark advance angle. Bargende [6] showed that the optimal spark advance is closely related to the angular position of the 50% mass fraction burned (MFB50) *i. e*. that optimal spark advance sets the MFB50 to be 8-10° CA aTDC. Mostly supported by experimental work and numerous testing, this conclusion has a logical theoretical background. Relying on the minimal entropy change analysis, during combustion, Beccari *et al.* [7] gave detailed explanation for the optimal position of MFB50. It is well known, that the ideal SI engine cycle assumes an instantaneous heat release in TDC, which is far from the process in a real engine. Even with neglecting the fact that the combustion duration is finite, by taking into account the heat losses during combustion, the angular position of the instantaneous combustion takes an important role in the indicated thermal efficiency (η_i).

The thermodynamically based analysis shows that the η_i can be improved by retarding the combustion process on account of lower temperatures and heat losses. Furthermore, Beccari *et al.* [7] demonstrated how to estimate this combustion angle delay in order to achieve the highest brake thermal efficiency (η_e) by taking into account the heat and friction losses during combustion, and that this estimate is in a good accordance with the simulations and the conclusions of Bargende [6].

A real combustion process is finite (not instantaneous), and this fact has the same effects on η_i as a lowering of the compression ratio. An asymmetry of the rate of heat release (ROHR) curve additional influences the efficiency. In order to place the ROHR curve centroid as close to the TDC, needed spark advance correction, with respect to TDC, equals the phase lag between the combustion duration symmetry line and centroid position [7]. Summed influences of heat transfer process, friction losses, combustion duration, and ROHR curve shape determines the optimal spark advance angle which leads to higher achievable brake thermal efficiency.

The concept of a combustion indicator based spark advance control is explained in fig. 1. The figure shows an example of measured in-cylinder pressure, ROHR and MFB curves (one of cycles from the regime No. 17, marked at the lower part off fig. 7). The presented example shows a cycle where the combustion process needs a delay, since the MFB50 indicator is out of the wanted, optimal angular span (8-10° CA aTDC). The ROHR is calculated as a differential of MFB and therefore is dimensionless, *i. e*. the rate represents the relative angular heat release increments.

The relation between the MFB50 position and spark advance angle is not straightforward. By changing the start of combustion angle, thermodynamic circumstances within the combustion chamber are changing also, thus affecting the whole combustion process. That means that the phasing of the spark advance causes not only the change in ROHR curve angular position but its shape too. Therefore, an advanced spark advance control system requires the feedback from the combustion process in order to maintain the highest achievable efficiency in real-time.

Today's SI engine control ignition system is map based and driven without a feedback in an so called open loop. Spark advance maps are defined during the process of engine calibration. Although the optimisation of the engine control parameters, during its calibration is very

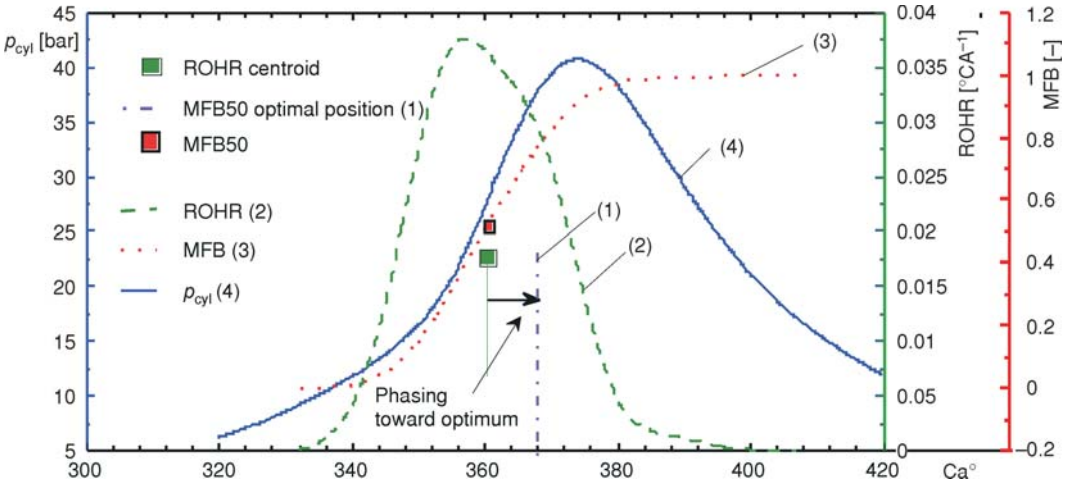

Figure 1. An example of the bad positioned combustion process which needs to be retarded in order to improve the cycle brake thermal efficiency

sophisticated and advanced, this open-loop type of control is unable to deliver the full efficiency potential through the engine lifetime. This is mainly caused by influences, which cannot be counted for during map calibration phase, like fuel characteristics variations or engine components aging factors. A modern concept of the spark advance control needs highly accurate information feedback, from the combustion process, in order to achieve optimal combustion efficiency. Therefore, they urge for some kind of sensor, which will provide the information on some crucial combustion features through its indicators, like MFB50, location of the peak in-cylinder pressure, location of the maximum pressure rise, *etc*. [8].

Combustion indicator, like MFB50, can be easily estimated by Rassweiler & Whitrow method from measured in-cylinder pressure [9, 10]. Whereas straightforward in extracting combustion features, this method has a major drawback in pressure sensor implementation costs and its durability. Alternative approaches are vastly investigated by researchers focusing on already available, common signals on SI engine, like ionisation current, engine block vibrations, and crankshaft angular speed. The angular speed and acceleration of the crankshaft, as a potential source of combustion indicators, has drawn far more attention among researchers because its availability and accessibility through a common engine speed measurement system. An angular speed of a crankshaft, which varies through a single engine cycle, is mainly formed by summing action of the gas torque T_g, originating from the in-cylinder gas pressure forces, and the mass torque T_m, caused by the oscillating parts of the engine. The information about the combustion process is contained in the gas torque and, consequently in the crankshaft angular speed. Although informative, the main obstacle, in using the angular speed as an effective combustion indicator source, is the high non-linear influence of the mass torque. Depending on the gas and the mass torque ratio, this influence can largely mask the information about the combustion process, contained in the angular speed signal. Furthermore, friction torques, originating from engine friction and external engine load torque also influence the angular crankshaft speed, but they are omitted from the focus of this work as less influencing factors.

The crankshaft is a complex and not an absolutely stiff object, subjected to highly variable load. This lead to torsional oscillations of the crankshaft segments and, depending on

the angular speed sensor placement, measured signal can be heavily influenced by this phenomenon, also. There are numerous approaches in solving these problems, but regardless of methods used, most of them are focused on the reconstruction of the in-cylinder pressure from the angular speed signal, as a first step in the signal analysis. Further analysis, as a second step, treats the reconstructed in-cylinder pressure as a measured one, and by using the common thermodynamically based methods, extract the combustion indicators.

This paper deals with the different two-step approach for obtaining the combustion indicator from the angular speed measurements. Relaying on relations between torques acting on the crankshaft, through the torque balance equation, first step transforms the angular acceleration to synthetic signal by freeing the original signal from mass torque influence. The second step is based on local linear neuro-fuzzy model (LLNFM) which uses this created synthetic signal as an input and estimates MFB50 combustion indicator directly, avoiding the in-cylinder pressure reconstruction step. Thus, this method has a potential for direct providing the closed loop spark advance control system with the MFB50 combustion indicator solely by measuring the angular speed of the crankshaft.

Synthetic torque variable

Crankshaft angular acceleration is built up by summing action of several torques: the aforementioned gas and mass torques (T_g and T_m), friction torque T_f and load torque T_l. The friction torque T_f originates from the friction forces within the engine and the load torque T_l acts as an external load, acting on the crankshaft and opposing the effective torque generated by the engine. These torques are related through the torque balance equation, which in general, for single cylinder takes the form:

$$J\theta'' = T_g(\theta) + T_m(\theta, \theta', \theta'') + T_f(\theta) + T_l(\theta) \tag{1}$$

where θ is the crank angle and J denotes the crankshaft's moment of inertia. Information on the combustion process is nested in in-cylinder pressure which is a part of the gas torque T_g:

$$T_g(\theta) = p_g(\theta) A_p \frac{ds}{d\theta} \tag{2}$$

where $p_g(\theta)$ is the in-cylinder absolute pressure, and A_p – the piston area and s denotes the piston displacement.

The mass torque evaluation is often based on the analysis of the kinetic energy of crankshaft mechanism modelled as two point mass system:

$$T_m(\theta, \theta', \theta'') = [-J_A(\theta) + m_B r^2]\theta'' - \frac{1}{2}\frac{dJ_A(\theta)}{d\theta}\theta'^2 \tag{3}$$

where the $J_A(\theta)$ is varying inertia of oscillating mass m_A with respect to the crankshaft axis, and m_B denotes the rotating mass on a crankshaft side (fig. 2). The exact expressions for the varying inertia and the derivatives of the piston displacement can be found in [11]. Non-linearity introduced by T_m in the eq. (1) is one of the main obstacles in establishing the straightforward linear relationship between angular speed θ' and in-cylinder pressure $p_g(\theta)$.

Since the mass torque $T_m(\theta)$ depends on design parameters of crankshaft mechanism (masses, moments of inertia,...) it is quite predictive and can be calculated in advance. Relaying on this idea, Moskwa *et al.* [12] suggested the method in which the whole mass torque is replaced by the product of the constant moment of inertia, and a new synthetic variable called synthetic angular acceleration. He used this method as a linearization technique for accessing the

combustion information through measured angular acceleration. Therefore, the term "synthetic", used in this paper, is an association on a paradigm for eliminating the inertia effects from the measured angular speed signal.

Schagerberg and Mckelvey [13] analysed the crankshaft model complexity influence on the estimation of combustion features using torque balance equation. Sometimes, model simplification can be justified but, in general, high-fidelity multi-body models lead to more accurate results. Since the crankshaft is a deformable, torsionally flexible object, its flexing and torsional vibrations affecting the angular speed signal. There are different approaches in the modelling of the crankshaft: from the simplest models, based on a single inertia mass to the complex multi-body models with included effects of variable inertia. Decision on how complex the crankshaft model should be, in order to give a satisfactory estimation of combustion features is related to the crankshaft modal shapes analysis [14]. When the harmonics of the first modal shape are very close to the engine operating speed regimes, self-amplified torsional vibrations cannot be neglected.

The model used in this paper, is a multi-body (lumped mass) based and takes the following matrix form:

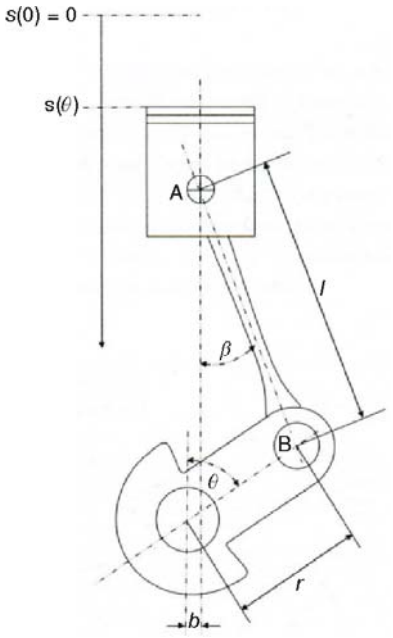

Figure 2. A crank-slider mechanism [10]

$$[\mathrm{J}][\theta''] + [\mathrm{C}][\theta'] + [\mathrm{K}][\theta] = [T_{\mathrm{g}}(\theta)] + [T_{\mathrm{m}}(\theta, \theta', \theta'')] + [T_l(\theta)] + [T_{\mathrm{f}}(\theta)] \tag{4}$$

where [J], [C], and [K] are the inertia, torsional damping and stiffness $N_{\mathrm{L}} \times N_{\mathrm{L}}$ symmetrical matrices, respectively. The values of crankshaft angular position, it's time derivatives and torques, in eq. (4), are vectors whose elements respond to N_{L} individual lumped masses of the model (fig. 3)

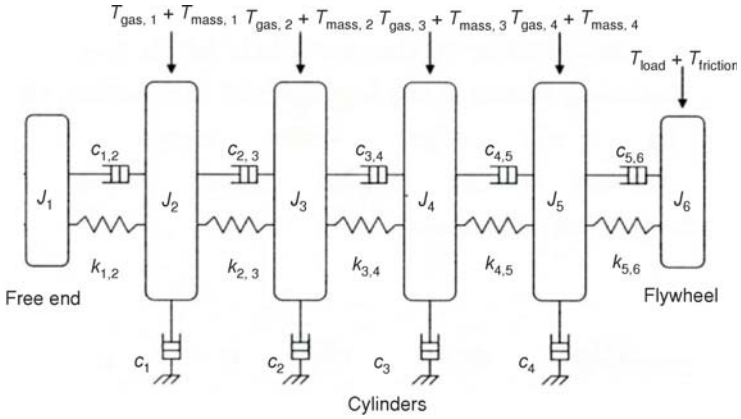

Figure 3. Torsional crankshaft lumped mass model for four cylinder engine

By assuming that the friction can be incorporated in damping loses, following variable can be defined:

$$T_{\text{synth}}(\theta) = \sum_{N}([\text{J}][\theta''_{\text{m}^*}] + [\text{C}][\theta'_{\text{m}^*}] + [\text{K}][\theta_{\text{m}^*}] - [T_{\text{m}}(\theta, \theta', \theta'')]) \tag{5}$$

This variable represents the estimate of the gas and the load torque sum and, knowing the parameters of the crankshaft model defined by eq. (4), can be calculated solely by means of measured crankshaft speed/acceleration where m^* subscript in eq. (5)). The variable T_{synth} contains complete information on combustion process. Since the variations of this variable are more influenced by the combustion process than load variation, this variable is a good candidate for combustion features estimation. The drawback of this approach and its prerequisite is the necessity for crankshaft model parameter identification. The next step, needed for estimating combustion feature from this variable, is the establishment of a model which is able to accurately correlate T_{synth} and MFB50. This model, as announced in the introduction, is neuro-fuzzy based and thus needs experimental data in order to be trained and tested. Therefore, gathering the experimental data is a very important step in accomplishing suggested combustion feature estimator.

LLNFM based virtual MFB50 sensor

Synthetic torque T_{synth}, calculated over the angular range at which combustion occurs, contains all relevant information about the combustion process. Relation between T_{synth} values and combustion feature like MFB50 is highly non-linear and depends on several complex processes, mainly the heat release and heat transfer process. Non-linearities are introduced by various, engine specific, parameters and circumstances derived from combustion chamber design, cylinder gas exchange processes, engine's working point, air-fuel ratio and so on.

The neural network models are featured by capabilities to establish functional approximation of the highly non-linear correlated data. Furthermore, their ability to learn from the existing data sets and to transform the contained knowledge into functional rules, distinguish them among other modelling techniques. The artificial neural networks, as universal function approximators, represent a computational paradigm based on the brain-like parallel processing [15-19].

By drawing the fuzzy models in a neural network based structure, hybrid neuro-fuzzy models can be created [20]. A neuro-fuzzy model combines the advantages of both modelling techniques: (1) The fuzzy models are not necessary designed by an expert knowledge but can be learned by data-driven process and (2) the identified rules are more interpretable than in neural networks models.

The advantage of LLNFM, in an approximation of a non-linear function, is their capability to model complex non-linearities by superposition of several very simple models – linear functions. Similar to fuzzification step in fuzzy models, the first step in defining LLNFM is partitioning of the input vector [u] and placing, locally valid, linear models. Validity of each linear model $L_i([\text{u}])$ is further defined by validation function $\Phi_i([\text{u}])$.

The output of the LLNFM is defined as:

$$\begin{aligned} y &= \sum_{i=1}^{M} L_i([\text{u}])\Phi_i([\text{u}]) \\ L_i([\text{u}]) &= \sum_{i=1}^{p} w_{i0} + w_{i1}u_1 + \ldots + w_{i\text{p}}u_{\text{p}} \end{aligned} \tag{6}$$

where M is the number of the local linear models and w_{ij} – the parameters of the i-th linear submodel, and $u_1 \ldots u_{\text{p}}$ – the elements of the input vector [u].

The validity function, often used, is a normalised Gaussian function in the form:

$$\Phi_i([\mathrm{u}], c_i, \sigma) = \frac{\Psi_i}{\sum_{k=1}^{M} \Psi_k}$$
$$\Psi_i = \exp\left\{-\frac{1}{2}\left[\sum_{j=1}^{p}\left(\frac{u_j - c_{ij}}{\sigma_{ij}}\right)\right]\right\} \tag{7}$$

where c_{ij} is the Gaussian function centre co-ordinate and σ_{ij} individual standard deviation for the j-th input and i-th model partition (submodel).

Structure of LLNF model, described by the eqs. (6) and (7), is shown in the fig. 4 (left). This model shares great similarity with the Tagaki-Sugeno fuzzy models and also can be interpreted as an extended normalised radial basis function (RBF) network, differing in the activation function weighting [20]. Whereas the RBF network neuron is weighted by single scalar, LLNFM neuron is weighted by a linear function. Input space partitioning and determination of local model parameters are driven by algorithms, which are data-driven – exactly the same as with neural networks.

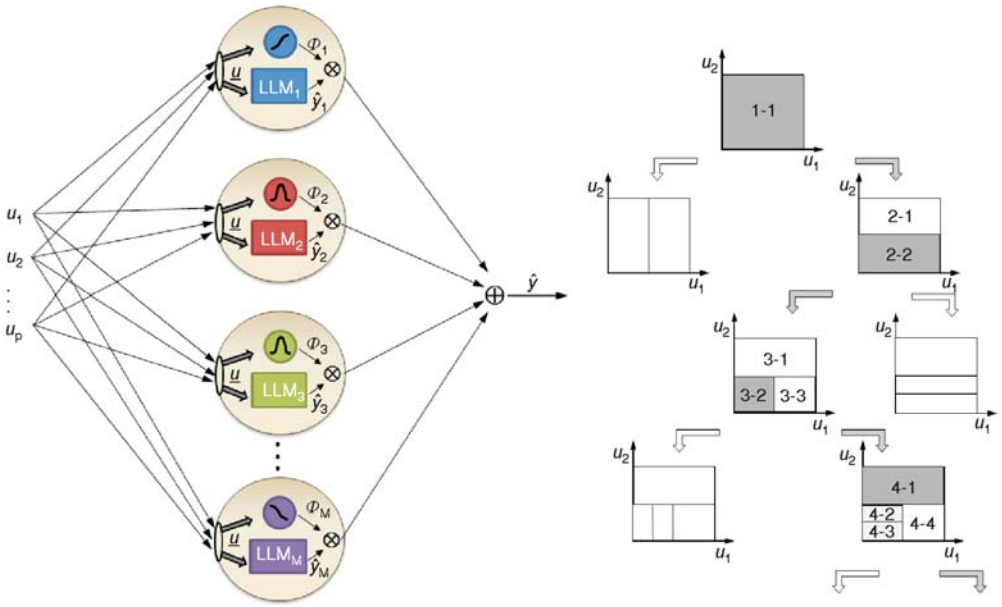

Figure 4. Network structure of a LLNFM with *M* submodels (neurons) for *p* inputs (left); Input space partitioning using Lolimot algorithm in the first four iteration for 2-D input space (*p* = 2)

The training algorithm used, named Lolimot (local linear model tree), is introduced by Nelles [20]. It divides the input space in so called (hyper-) rectangles. Upon each division, local linear models are placed in each of the parted spaces. Depending on the modelling error, the algorithm makes the decision how to perform the input space division in further iterations (fig. 4, right). It works as an incremental tree-construction, input space partitioning algorithm. The way the input space is partitioned, and location of linear models gives this LLNFM a great

interpretability, especially when the number of inputs is low [21]. In order to adapt the width of each Gaussian function to the width of partitioned space Δ_{ij}, each Gaussian width is calculated as $\sigma_{ij} = \sigma_L \Delta_{ij}$, where σ_L is globally set parameter for entire LLNFM.

The simplest way to implement the LLNFM is to use this model as a MISO model, which is perfectly suited for deriving single scalar as an output from the multiple inputs. In order to take into account the parameters, which significantly influence the combustion process, cycle averaged pressure in the intake manifold $\overline{p}_{im}$ and the cycle averaged crankshaft speed $\overline{n}_{eng}$ are added to the input vector which takes the form:

$$[u]^{(i)} = [T^{(i)}_{synth,\,map}, \overline{n}^{(i)}_{eng,\,map}, \overline{p}^{(i)}_{im,\,map}] \tag{8}$$

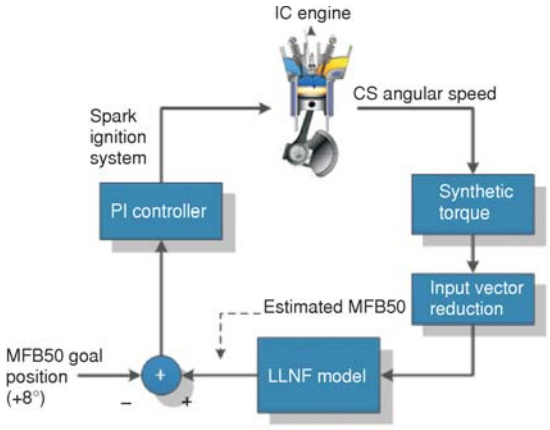

Figure 5. Two-step concept of closed loop spark advance control implementing virtual LLNFM based MFB50 sensor

where (i) designates each engine cycle. All three signals, comprising the input vector, are mapped into the range [–1, 1].

The output of the LLNFM is the MFB50 combustion indicator:

$$y^{(i)} = \mathrm{MFB50}^i \tag{9}$$

One of advantages of LLNFM is their capability to model non- linearities with a relatively small number of neurons and therefore, they have a potential to be implemented in fast real-time spark advance control algorithms. Complete closed-loop control, with synthetic torque evaluation step, is presented in the fig. 5.

Measurement set-up and data acquired

The engine used, as an experimental object, is described in the tab. 1. The measurement is set up so to provide data for two separate analysis tasks (fig. 6). The identification of parameters of the crankshaft model requires measurement of the crankshaft angular speed. It was accomplished by means of an optical incremental encoder mounted at the free end of the crankshaft. A higher encoder resolution is more appropriate to this type of measurements (*e. g.* 0.1° CA), but lack of one forced usage of an available 1° CA resolution encoder. Simultaneously, in-cylinder pressure was measured by means of piezoelectric, water cooled pressure sensor. Both signals, measured in the angular domain, were crucial for preparing input (T_{synth}) and output (MFB50) training and test data sets for Neuro-fuzzy virtual sensor model.

Table 1. The engine data

Manufacturer	DMB
Type	4 cylinder inline 4 stroke SI; 2 valves per cylinder
Firing sequence	1-3-4-2
Bore [mm]	80.5
Stroke [mm]	67.4
Conrod length [mm]	128.5
Piston pin offset [mm]	3.6
Compression ratio [–]	9.03

Anticipated accuracy of LLNFM is related to the amount and the quality of

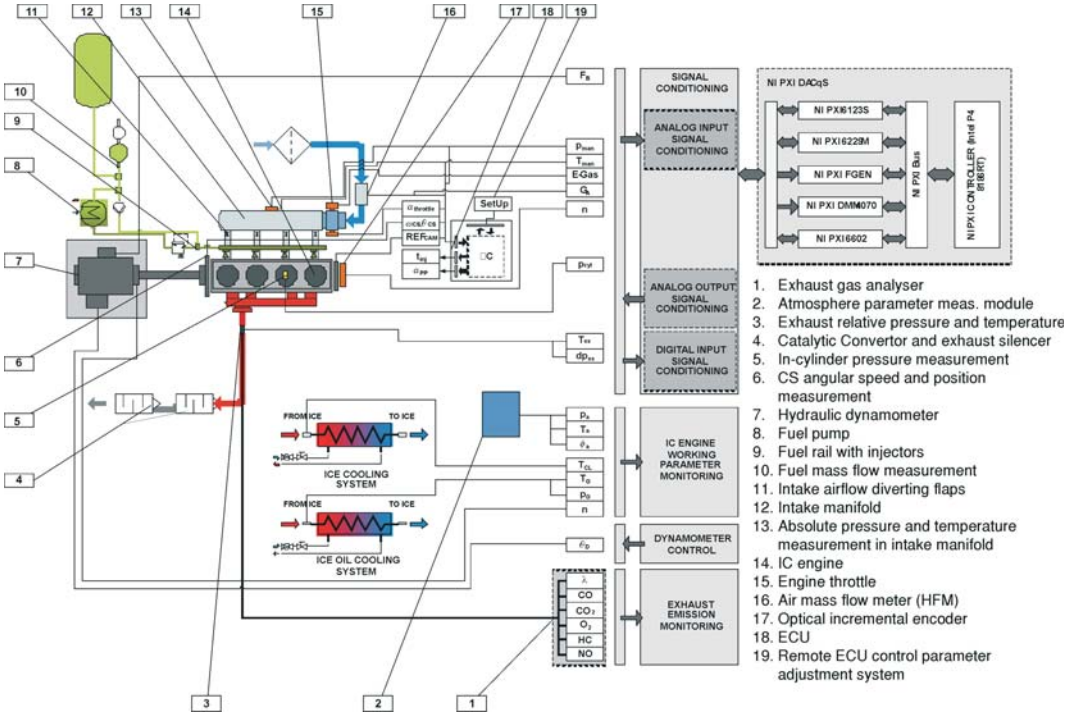

Figure 6. IC Engine test bed with instrumentation and control systems (FME ICED Lab)

the data acquired for its training and testing. The engine was equipped with the laboratory prototype of a variable induction system (VIS). This system [22] had an ability to influence the intake port airflow, when turned on, which consequently, affected the combustion process. For that reason, this system was used in order to almost double the number of engine's working points by simply turning that system on (VIS-on) or off (VIS-off).

Totally, 141 engine's working points were recorded with 50 cycles each, which gave more than 7000 input-output pairs of data for LLNFM training and testing (fig. 7). Ought to mention that this number is not impressive in the world of IC engine neural models data gathering, but it was limited because of specific restrictions found on the engine used on a test bench (particularly limitation of maximum engine speed).

Data analysis and preparation

Since the accuracy of measured signals has the key influence on usability of created models, full attention is paid to the correction of the measured angular speed due to mechanical imperfections of the measurement system [23, 24].

By conducting in-depth analysis of burn rate evaluation routines, Brunt and Emtage [25] concluded that the evaluation of MFB50 is very sensitive to in-cylinder pressure referencing errors and errors in TDC determination. In order to minimise these errors measured raw in-cylinder data are treated very carefully. In-cylinder pressure data are referenced using the technique described by Hohenberg [26], on a limited angular interval (100º-65º CA bTDC).

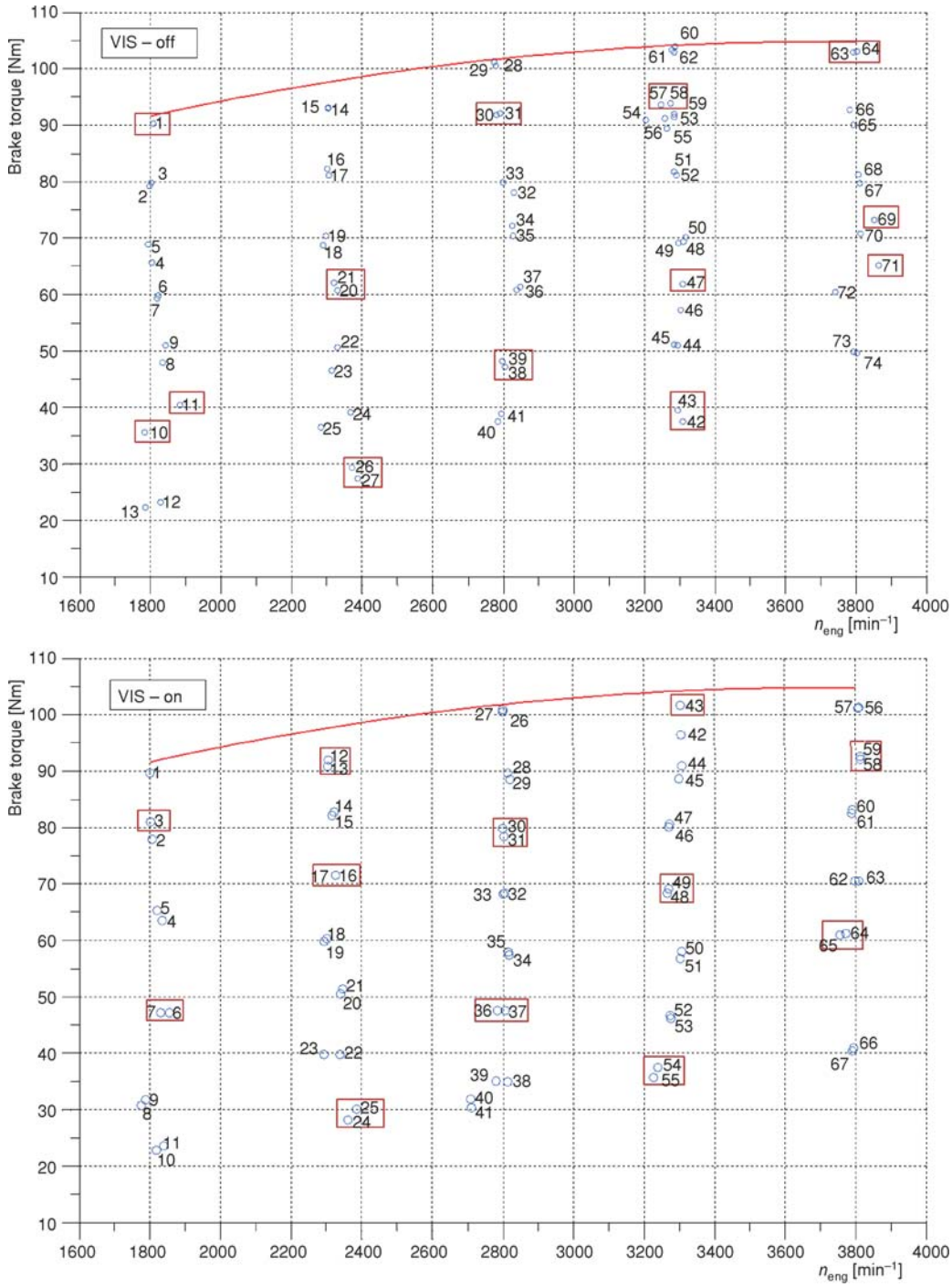

Figure 7. Map of recorded stationary engine's regimes with VIS on (above) and VIS off (below). Regimes, marked with rectangles, are separated for LLNFM training (cm^3 30%). The rest of the data are used for model testing (~70%)

Since the measured intake plenum pressure was also available, as suggested by Brunt and Pond in [27], these values were used for an initial in-cylinder pressure offset.

The TDC position and the compression ratio, as well, are the factors which largely affect the accuracy of all in-cylinder pressure derived conclusions. Correct TDC position and compression ratio are determined by the method described by Tazerout *et al.* [28], which is based on the *T-s* (entropy – temperature) diagram peak shape and symmetry analysis. Because of its importance, determined TDC position is checked also by the thermodynamically based method, proposed by Tunestal [29] which confirmed a good agreement with the *T-s* shape and loop method (within 0.1º CA).

Correctly positioned in-cylinder pressure further provided the base for calculation of MFB curve and determination of MFB50 position for each of the measured engine cycles which will be used as targets in training and validation process of LLNFM. Calculation of the burn rate is closely related to heat release and heat transfer process during combustion. The method proposed in [30] is simple and straightforward despite its incorporated heat transfer model. However, most of publications discussing the spark advance, MBT and MFB50 relations, as well as their conclusions, are based on Rassweiler & Whitrow (R&W) method for the burn rate calculation [9]. Therefore, the method used in this paper will be also based on R&W method, but slightly improved by Shayler [10].

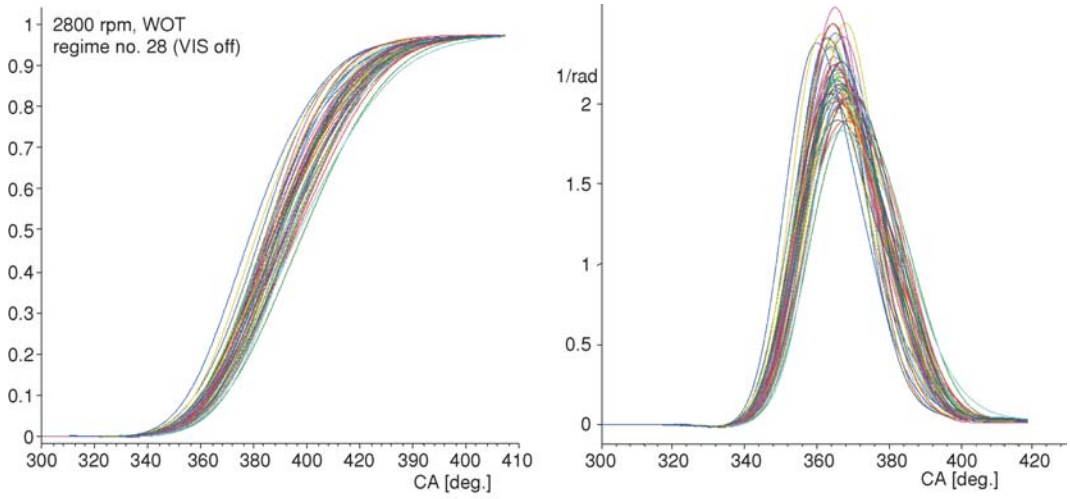

Figure 8. Typical results of MFB curve calculation (left) and its derivative (right); 50 consecutive cycles

R&W method is based on extracting the pressure rise due to combustion, Δp_c from the start of combustion to the estimated end of combustion. Whereas the original R&W method assumes the values of compression and expansion process polytropic coefficients, improved method checks their values by evaluating the calculated Δp_c near the start and the end of combustion. The process is iterative, and when the values of polytropic coefficients lead to almost zero pressure rise near these points, the polytropic coefficient identification process stops. The identified polytropic coefficient for the compression process is used in the MFB calculation till the TDC, and the expansion process coefficient afterwards (fig. 8).

Model parameter identification

Re-arrangement of eq. (4) and separation of terms in eq. (3) leads to second-order differential equation of motion of the crankshaft:

$$[\mathrm{J}(\theta)][\theta''] = -[\mathrm{C}][\theta'] - [\vec{\mathrm{K}}][\theta] + [T_{\mathrm{g}}(\theta)] + [T_{\mathrm{m_2}}(\theta,\theta')] + [T_{\mathrm{l}}(\theta)] + [T_{\mathrm{f}}(\theta)] \tag{10}$$

where the varying inertia is the term multiplying θ'' in eq. (3):

$$[\mathrm{J}(\theta)] = -[\mathrm{J_A}(\theta)] + m_{\mathrm{B}} r^2 + [\mathrm{J}] \tag{11}$$

and the mass moment $T_{\mathrm{m_2}}$ is the part of eq. (3) which depends on the angular speed:

$$[T_{\mathrm{m_2}}(\theta,\theta')] = -\frac{1}{2}\frac{\mathrm{d}J_{\mathrm{A}}(\theta)}{\mathrm{d}\theta}\theta'^2 \tag{12}$$

Equation (10) can be further transformed to the system of two first-order equations. This system is stiff, by its nature, and require the stiff system solver which is able to handle separate calculation of mass function $J(\theta)$. A good example of such a solver is Matlab® ode23tb function. The in-line four cylinder crankshafts can be modelled as a system of six lumped masses interconnected with torsional damper and spring elements, which is shown in fig. 3. That in start gives 16 unknown parameters which should be identified (five stiffness and five damping coefficients; six moments of inertia).

By comparing the simulated ($[\theta''_{\mathrm{sim}}]$) and measured ($[\theta''_{\mathrm{meas}}]$) angular acceleration error function F can be formulated:

$$F([p_{\mathrm{S}}]) = [[\theta''_{\mathrm{meas}}] - [\theta''_{\mathrm{sim}}([p_{\mathrm{S}}])]^T [\theta''_{\mathrm{meas}}] - [\theta''_{\mathrm{sim}}([p_{\mathrm{S}}])]] = [\varepsilon]^T [\varepsilon] \tag{13}$$

with $[p_{\mathrm{S}}]$ as a vector containing not yet identified parameters. This function can be successfully minimised by means of Levenberg-Marquardt algorithm. When the parameters of the crankshaft model are identified it is possible to apply eq. (5) and calculate the synthetic torque variable.

Examples of calculated signals T_{synth}, are shown in fig. 9. The disturbances, which are noticeable on higher engine speed, especially on descending side of the signal, indicate that mass torque influence is not completely vanished. This is mainly a consequence of a fairly simple approach in the modelling of the friction torque. However, within the angular window in which combustion occurs, these anomalies are hardly visible. The focus of the analysing window is in 40° before and after TDC where the complete combustion mainly occurs.

The calculated T_{synth} values are further prepared for the placement in the LLNFM input vector by mapping its input range to the interval [–1, 1]. The examples of the mapped versions of the synthetic torque variable are shown in fig. 10, with corresponding mapped versions of the MFB curves. The signals are presented in the angular window [–40º…+40º] CA aTDC, same as in fig. 9.

The key parameters, determining the performance of the LLNFM are the number of local linear models (neurons) M, and the Gaussian function width, given via parameter σ_{L}. In order to find the optimal values of these parameters several numerical tests were conducted by varying number M in range [2…7] and σ_{L} in range [0.2…0.5]. The performance indicator used, was the standard deviation of MFB50 estimating error:

$$\sigma_{\Delta_{\mathrm{MFB50}}} = \sqrt{\frac{1}{N-1}\sum_{N}(\Delta_{MFB50} - \overline{\Delta}_{MFB50})} \tag{14}$$

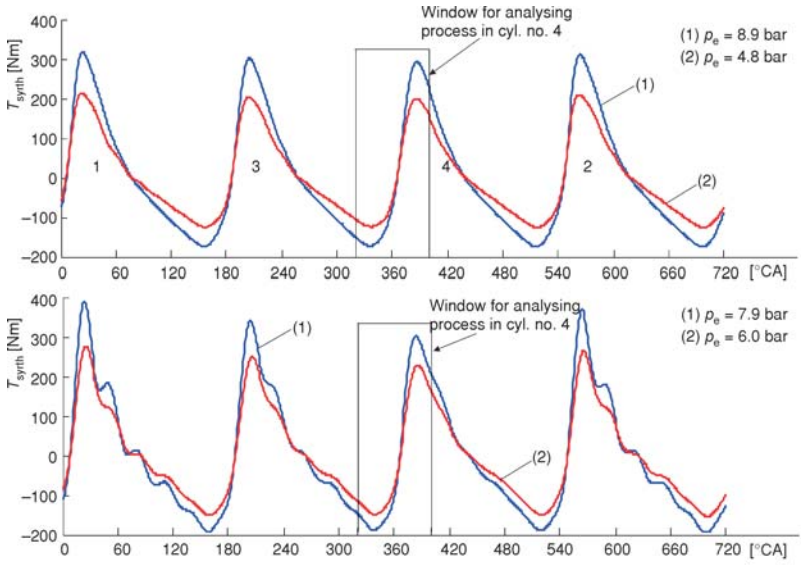

Figure 9. Examples of calculated T_{synth} on 1800 and 2300 rpm on full (1) and partial load (2)

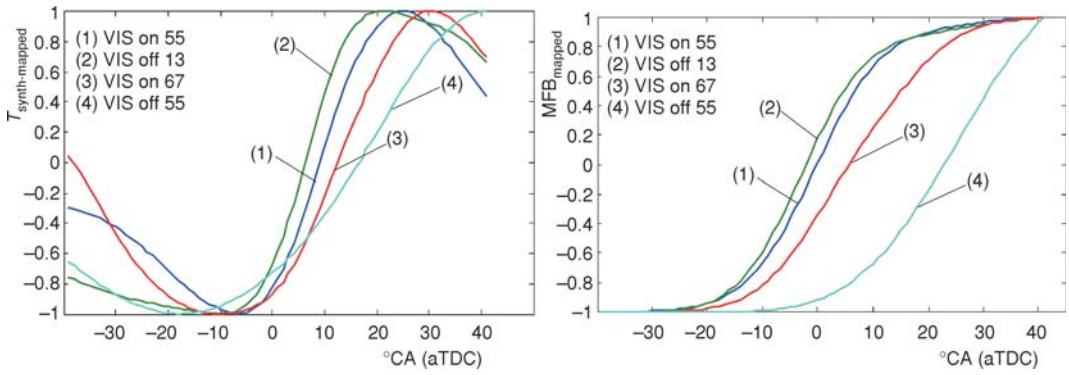

Figure 10. Mapped T_{synth} and corresponding MFB curves for several picked regimes and cycles; regimes can be tracked, through its designation in fig. 7

where N is the number of input vectors available for training/validation (number of engine cycles). Estimating error is defined as:

$$\Delta_{MFB50} = MFB50_{sim} - MFB50_{measured} \tag{15}$$

Testing with the full-length input vector containing T_{synth} with 81 elements (1°CA resolution on [–40…+40]°CA span around TDC), showed that the vector length can be reduced without significantly affecting the LLNF model performance. Taking into account T_{synth} with 6° CA resolution, size of the LLNFM input vector (eq. (8)), can be significantly reduced by employing 15 instead of 83 elements ($13 \times T_{synth\ map} + \overline{n}_{eng.\ map} + \overline{p}_{im.\ map}$).

Table 2. Results of numerical tests of different LLNFM configurations – values of $\sigma_{\Delta_{MFB50}}$ on test data set (5000 cycles) in °CA

M↓ \ σ_L→	0.2	**0.24**	0.3	0.4	0.5
2	0.400	0.405	0.414	0.445	0.447
3	0.392	0.382	0.391	0.385	0.496
4	0.369	0.357	0.419	0.353	0.576
5	0.353	**0.332**	0.389	0.351	0.610
6	0.581	0.340	0.452	0.379	0.590
7	0.597	0.341	0.486	0.385	0.585

The results of numerical tests are shown in tab. 2, with bolded values of parameters leading to lowest value $\sigma_{\Delta_{MFB50}}$. Each of the LLNFM configurations is learned on the learning data set and then tested on the, more than twice larger, test data set. A relatively low values of $\sigma_{\Delta_{MFB50}}$, on test data set, indicates the very good performance and generalization capabilities of the created LLNFM.

Cycle-by-cycle variations are common in SI engines. Pipitone [8] concluded, that combustion features, extracted in cycle-by--cycle manner and used as an input in a spark advance control system, can cause very large fluctuations of this control variable (±10° CA). In order to avoid this, and provide the spark advance control system with the more stable combustion indicator, its value should be averaged.

Pipitone also showed that for the MFB50 indicator, the minimum number of engine cycles for stable indicator evaluation is strongly dependent on IMEP COV, with the conclusion that the mean value of the minimum number of cycles is around 14. Having this in mind, resulted output vector of the LLNFM is averaged by moving average filter (fourteen cycle width), and performance indicators are calculated over this smoothed MFB50 output.

A variation of the error Δ_{MFB50}, in estimating the MFB50 combustion indicator on the test data set, is shown in fig. 11. It is clear that the performance of the LLNFM used, suffers on

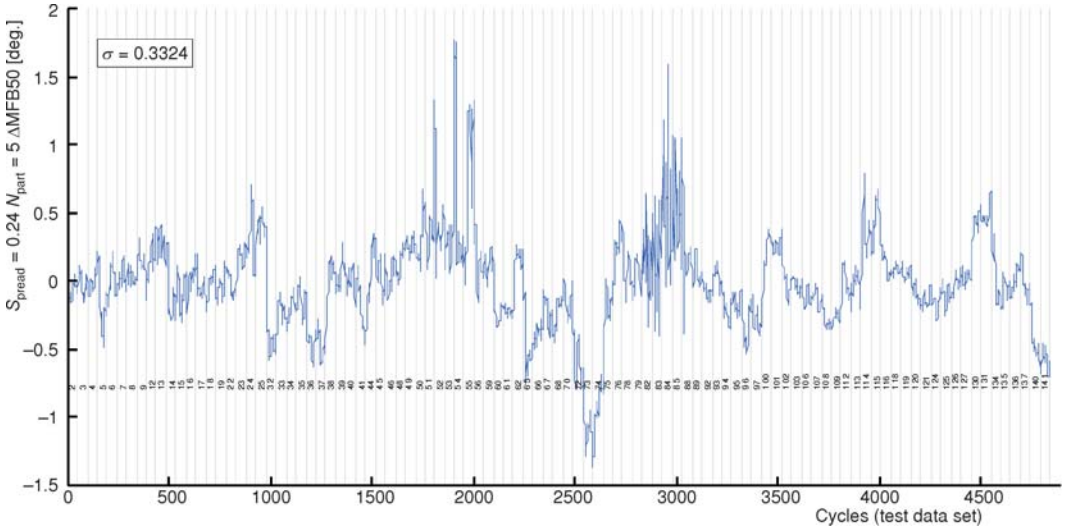

Figure 11. Δ_{MFB50} variation on the test set [°CA], LLNFM σ_L = 0.24, M = 5

some cycles with MFB50 estimation error exceeding more than 1° CA. Most of these cycles belong to the partial load regimes, driven with the leaner air-fuel mixture, where partial combustions and misfires are not uncommon. This implies that the air to fuel ratio (AFR), as an additional element in the LLNFM input vector $\underline{u}$, could improve the model performance. This AFR feedback can be taken from wideband λ exhaust gas oxygen sensor. Since the λ sensor response is delayed, its implementation in the model would require the use of a more complex dynamic LLNFM. On the other hand, designed static LLNFM performance can be improved by filtering and eliminating the misfired cycles from processing. This can be achieved, *e. g.*, by the implementation of the effective CASMA filter [31].

Pipitone also concluded that acceptable variation of an estimated MFB50 indicator can be as high as ±1.63°CA in order to maintain the spark advance within the ±1.8°CA, which consequently influences the efficiency loss with an acceptable mean of 0.2%. In order to evaluate the performance of LLNFM, variation of the estimated MFB50 values should be compared with that limits. By assuming that the almost whole span of estimated values is in the range of $(2\ldots3)\sigma_{\Delta_{\mathrm{MFB50}}}$, an acceptable variation of the LLNFM MFB50 estimation should be:

$$\sigma_{\Delta_{\mathrm{MFB50}}} < 0.54°\mathrm{CA} \tag{16}$$

which means that the constructed LLNFM has enough accuracy (see tab. 2), and can be potentially used in a closed loop spark advance control systems, even without discussing the above-mentioned misfire or partial combustion problems.

Created LLNFM is a compact five neuron model with stored 5×16 coefficients. Non-optimised code (MFB50 estimation) execution speed, in Matlab® environment takes approx. 10 μs of CPU time on a desktop PC with Intel I7-920 processor. In order to ensure its performance on slower automotive microcontroller or DSP platforms some effort should be made in the implementation of the input vector reduction techniques which can lead to more than halved execution times. Some of them, like principal component analysis (PCA), are widely used, but other approaches, like one based on the mutual information concept, seems particularly promising and applicable [32].

Conclusions

The spark advance is one of the key parameters affecting the combustion efficiency in an SI engine. In order to accomplish the optimal combustion efficiency, closed loop spark advance control system is needed, which requires accurate information on a combustion process. The combustion process feedback, based on the in-cylinder pressure analysis is straightforward, but it has its drawback, which delays the production line implementation. As an alternative to the direct in-cylinder pressure measurement, an alternative approach is suggested, and method developed, employing software based virtual combustion indicator sensor. The proposed sensing system estimates MFB50 combustion feature by calculating so called synthetic torque, and transforming it to MFB50 value through a nonlinear estimator based on local LLNFM.

Calculation of the synthetic torque is based on the identified parameters of a high fidelity calibrated dynamic model of the crankshaft. The synthetic torque signal contains high-quality information on the combustion process with negligible mass torque influence easing the combustion process information access. LLNFM, trained on the 30% and tested on 70 % of acquired experimental data, demonstrated very good performance in estimating the MFB50 with excellent generalization capabilities. The LLNFM input vector, based on the synthetic torque signal, averaged cycle engine speed and intake manifold pressure, provides enough information for the highest quality training of the LLNFM. The model testing showed that the model is prone

to generate increased errors in the MFB50 estimation on low load or idle engine regimes, mainly because of a misfire and partial combustion caused by a leaner air-fuel mixture used. Despite this fact, designed LLNFM outperforms the minimum allowable error variation and provides acceptable input for the closed-loop spark advance control system.

The reduction of the input vector size, by reducing the angular resolution of the synthetic torque variable, enabled the compact design of the LLNF model with only five neurons. Further reduction of the LLNFM input vector, based on the information content extraction, could lead to the additional model size reduction and processing requirements, which can be acceptable to the modern real time engine control units.

Acknowledgments

The authors would like to acknowledge Slobodan Popović (Faculty of Mechanical Engineering, ICE Department) for his support and technical suggestions in the development of this work.

Acronyms

AFR – air to fuel ratio
aTDC – after top dead centre
bTDC – before top dead centre
CA – crankshaft angle
CASMA – crank angle synchronous moving average
COV – coefficient of variation
CPU – central processor unit
DSP – digital signal processor
IC – internal combustion
IMEP – indicated mean effective pressure
LLNFM – local linear neuro-fuzzy model
MBT – maximum brake torque
MFB50 – angular position of the 50% of mass fraction burned
MISO – multiple input single output
PCA – principal component analysis
RBF – radial basis function
ROHR – rate of heat release
SI – spark ignition
TDC – top dead centre
VIS – variable intake system

References

[1] ***, CO_2 Emissions from Fuel Combustion 2011 – Highlights, International Energy Agency, Paris, 2011
[2] ***, Regulation (EC) No 443/2009 of the European Parliament and of the Council Setting Emission Performance Standards For New Passenger Cars as Part of the Community's Integrated Approach to Reduce CO_2 Emissions from Light-Duty Vehicles (Text with EEA Relevance), European Commission, 2009
[3] Heywood, J. B., Internal Combustion Engine Fundamentals, McGraw-Hill, New York, USA, 1988
[4] Rakopoulos, C. D., Giakoumis, E. G., Second-Law Analyses Applied to Internal Combustion Engines Operation, *Progress in Energy and Combustion Science, 32* (2006), 1, pp. 2-47
[5] Teh, K.-Y., Miller, S. L., Edwards, C. F., Thermodynamic Requirements for Maximum Internal Combustion Engine Cycle Efficiency. Part 1: Optimal Combustion Strategy, *International Journal of Engine Research, 9* (2008), 6, pp. 449-465
[6] Bargende, M., Most Optimal Location of 50% Mass Fraction Burned and Automatic knock Detection, *MTZ, 56* (1995), 10, pp. 632-638
[7] Beccari, A., *et al*., An Analytical Approach for the Evaluation of the Optimal Combustion Phase in Spark Ignition Engines, *J. Eng. Gas Turbines Power, 132* (2010), 3, pp. 032802-032812
[8] Pipitone, E., A Comparison between Combustion Phase Indicators for Optimal Spark Timing, *Journal of Engineering for Gas Turbines and Power, 130* (2008), 5, pp. 052808-052818
[9] Rassweiler, G. M., Withrow, L., Motion Pictures of Engine Flames Correlated with Pressure Cards, SAE paper 380139, 1938
[10] Shayler, P. J., *et al*., Improving the Determination of Mass Fraction Burnt, SAE paper, 900351, 1990
[11] Maass, H., Torques in Internal Combustion Engines and their Balancing, Springer, Wien, 1981
[12] Moskwa, J. J., *et al*., A New Methodology for Use in Engine Diagnostics and Control, Utilizing 'Synthetic' Engine Variables: Theoretical and Experimental Results, *Journal of Dynamic Systems, Measurement, and Control, 123* (2001), 3, p. 528

[13] Schagerberg, S., Mckelvey, T., Instantaneous Crankshaft Torque Measurements – Modeling and Validation, SAE paper 2003-01-0713, 2003
[14] Ponti, F., Development of a Torsional Behavior Powertrain Model for Multiple Misfire Detection, *J. Eng. Gas Turbines Power, 130* (2008), 2, pp. 022803-022815
[15] Miljkovic, Z., Aleksendric, D., Artificial Neural Networks – Solved Examples with Short Theoretical Background (in Serbian), Faculty of Mechanical Engineering, University of Belgrade, Belgrade, 2009
[16] Haykin, S. S., Neural Networks: A Comprehensive Foundation, Macmillan, New York, USA, 1994
[17] Kalogirou, S. A., Artificial Intelligence for the Modeling and Control of Combustion Processes: A Review, *Progress in Energy and Combustion Science, 29* (2003), 6, pp. 515-566
[18] Van Der Smagt, P. P., Krose, B. J. A., An Introduction to Neural Networks, 8th ed., The University of Amsterdam, Amsterdam, The Netherlands,1993
[19] He, Y., Rutland, C. J., Application of Artificial Neural Networks in Engine Modelling, *International Journal of Engine Research, 5* (2004), 4, pp. 281-296
[20] Nelles, O., Nonlinear System Identification: from Classical Approaches to Neural Networks and Fuzzy Models, Springer, Berlin, 2001
[21] Müller, N., Hafner, M., Isermann, R., A Neuro-Fuzzy Based Method for the Design of Combustion Engine Dynamometer Experiments, SAE paper 2000-01-1262, 2000
[22] Tomić, M., *et al*., Dual Port Induction System for DMB 1.4MPI Engine, *Proceedings*, DEMI 2011, Banja Luka, Bosnia and Herzegovina, 2011, pp. 651-659
[23] Kiencke, U., Eger, R., Messtechnik: Systemtheorie für Elektrotechniker (Measurement: Systems Theory for Electrical Engineers – in Germany), Springer, Berlin, 2008
[24] Fehrenbach,H., *et al.*, Inservice Compensation of Sensor Wheel Tolerance, *MTZ, 63* (2002), 7/8, pp. 588-591
[25] Brunt, M. F. J., Emtage, A. L., Evaluation of Burn Rate Routines and Analysis Errors, SAE paper 970037, 1997
[26] Hohenberg, G. K., Basic Findings Obtained from Measurement of the Combustion Process, *Proceedings*, 19th International Fisita Congress, Melbourne, Australia, 1982, SAE paper 82126, pp. 126.1-126.8
[27] Brunt, M. F. J., Pond, C. R., Evaluation of Techniques for Absolute Cylinder Pressure Correction, SAE paper 970036, 1997
[28] Tazerout, M., *et al.*, Compression Ratio and TDC Calibrations Using Temperature- Entropy Diagram, SAE International, SAE paper 1999-01-3509, 1999
[29] Tunestal, P., TDC Offset Estimation from Motored Cylinder Pressure Data Based on Heat Release Shaping, Oil & Gas Science and Technology – *Revue d'IFP Energies Nouvelles, 66* (2011), 4, pp. 705-716
[30] Tomić, M., *et al*., A Quick, Simplified Approach to the Evaluation of Combustion Rate from an Internal Combustion Engine Indicator Diagram, *Thermal Science, 12* (2008), 1, pp. 85-102
[31] Schmidt, M., *et al*., Combustion Supervision by Evaluating the Crankshaft Speed and Acceleration, SAE paper 2000-01-0558, 2000
[32] Heister, F., Nonlinear Feature Selection Using the General Mutual Information, Ph. D. thesis, Johann Wolfgang Goethe-University, Frankfurt on the Main, Germany, 2008

Paper submitted: July 3, 2012
Paper revised: September 6, 2012
Paper accepted: September 16, 2012